MODELING THE IMPACT OF POST-FLASHOVER SHIPBOARD FIRES ON ADJACENT SPACES

Derek A. White, Craig L. Beyler, and Joseph L. Scheffey
Hughes Associates, Inc.
Baltimore, MD

Frederick W. Williams
Naval Research Laboratory, Washington, DC

ABSTRACT

Post-flashover fires in shipboard spaces have pronounced effects on adjacent spaces due to highly conductive boundaries. A model has been developed which predicts the thermal environment in such spaces. The model is based on radiative and convective heat transfer involving the hot wall (common boundary between post-flashover and adjacent space), the cold walls, and a gray gas. This theoretical description is reduced to a set of simultaneous non-linear equations that are solved by a Newton-Rapheson method. Experimental data provided the input function for the hot wall, and the model predictions for the gas temperature and the cold wall temperature have been compared with the experimental data. The comparisons shown are conservative, but representative, in accordance with modeling assumptions.

INTRODUCTION

Post-flashover compartment fires have been thoroughly studied and well characterized.[1-11] As reported in the literature, mathematical models have been developed to predict temperature histories in a post-flashover compartment,[12-16] and computer models have been established that implement mathematical models.[17] Shipboard compartments present unique challenges as a result of the construction and materials used. Post-flashover fires in shipboard compartments have been investigated.[18-22] Highly conductive boundary materials that are very thin, i.e., uninsulated steel bulkheads, result in substantial heating of adjacent spaces. A model which would predict the thermal impact of post-flashover fires on adjacent compartments (not connected by openings) would be very useful in the context of hazard analysis and the development of shipboard firefighting doctrine. Hazard analysis in terms of tenability, ignition of Class A materials (ordinary combustibles), and the thermal environment exposing sensitive equipment are important issues to address.

Limited efforts describing mathematical modeling of the environment in a compartment adjacent to a post-flashover shipboard compartment are available in the literature.[23] These efforts used the CFAST model to predict vertical heat transfer in several compartments removed from the fire.[23] Reasonable agreement between the predicted and experimental results was achieved, but results were limited to vertical heat transfer. The work reported herein, unrelated to that in Ref. 23, has been responsible for the development of a heat transfer algorithm that models the radiative and convective heat exchange affecting an adjacent (vertical or horizontal) space.

The model is based on a theoretical heat transfer description of the energy gains and losses in the space. The energy gains stem from a hot steel boundary which is common between the post-flashover compartment and the compartment of interest. Energy losses are those attributed to convection and radiation between the other steel surfaces and the ambient surroundings. The model was initially developed with parameters (convective heat transfer coefficients and surface emissivities) based on engineering calculations and literature values. Initial model comparisons against intermediate-scale experimental investigations[18-19] were used to refine parameter values.

These comparisons were used to validate the model and provided a foundation to set final parameter values. Applicability of the model to full-scale shipboard configurations was determined through comparison of model predictions to full-scale test data[22] from experiments performed on the US Navy fire research ship,[24] ex-USS SHADWELL. These were blind predictions that used unmodified, final model parameters developed from the reduced-scale comparisons.

Theoretical Development

A model that predicts the impact of a post-flashover shipboard fire on the thermal environment in an adjacent space was developed based on heat transfer principles. The "hot" wall boundary is characterized by a single temperature and is an input parameter prescribed by the modeler. The time-temperature history of the hot wall drives the model predictions for any given scenario as it is the single factor that determines the quantity of heat that can be transferred into the adjacent space. The time-temperature history can be predicted using a modified version of COMPF2.[17,25] Alternatively, functions describing experimental data can be used.

The attributes of the adjacent space that impact the heat transfer exchange description are defined in the following manner. The adjacent space is considered to be a closed compartment with no vent. However, leak areas are assumed to be sufficient to avoid any pressure increase as a result of the temperature rise. The gas in the adjacent compartment is assumed to be a well-stirred, uniform mixture that can be characterized by a single temperature. This assumption was motivated by experimental results that showed a thermal gradient as opposed to distinct thermal stratification.[18-19] Radiatively, this homogenous gas was considered to be a gray gas. This allows for simulating various gas characteristics from transparent to black, which could arise from smoke leakage into the adjacent space or from paint or other materials pyrolzying on the "hot" boundary.

The compartment boundaries are treated as thermally thin. The common boundary between the post-flashover space and the adjacent compartment is treated as the hot boundary, which has associated heat transfer parameters. The remaining five boundaries are characterized as a single "cold" boundary. The cold boundary heat transfer parameters and cold boundary temperature represent average values for the five remaining boundaries.

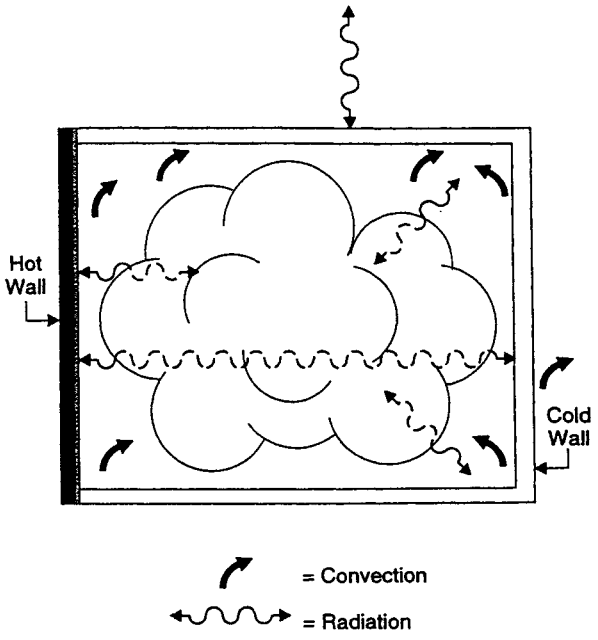

Figure 1. Modes of heat transfer modeled.

The impact on the thermal environment is modeled by several distinct heat transfer interactions between the four participants: the hot boundary, the cold boundary, the gray gas, and the ambient atmosphere outside the adjacent compartment. Figure 1 illustrates the control volume representation of the adjacent compartment with the heat transfer exchanges identified. Figure 1 shows the space with a gray gas participating in the radiant exchange. There is radiant heat transfer between the gray gas and both the hot boundary and cold boundary, between the cold boundary and the ambient surroundings, as well as from the hot boundary to the cold boundary. Convective heat transfer between the hot boundary and the gas in the compartment, between the compartment gas and the cold boundary, and between the cold boundary and the ambient surroundings are included in the model.

An energy balance for the gas in the adjacent space, which includes convective gains and losses as well as radiation absorption and emission, is given by

$$\frac{d}{dt}(\rho V C_p T_{gas}) = h_h A_h (T_h - T_{gas}) - h_c A_c (T_{gas} - T_c) + \frac{J_h - E_g}{R_4} + \frac{J_c - E_g}{R_5} \quad (1)$$

If it is assumed that the room has sufficient leakage to avoid a pressure increase and that the air density is inversely proportional to its temperature, the energy content of the air (gases) in the space will not change.[26] It may seem counterintuitive that the compartment volume becomes irrelevant. Equation 1 can then be reduced to the following:

$$h_h A_h (T_h - T_{gas}) - h_c A_c (T_{gas} - T_c) + \frac{J_h + E_g}{R_4} + \frac{J_c - E_g}{R_5} = 0 \quad (2)$$

The cold boundary is also thermally thin and, as such, has been considered as a lumped mass. Applying the conservation of energy to the cold boundary, a differential equation for the cold boundary temperature is written.

$$A_c \Delta_x \rho C_p \frac{dT_c}{dt} = \frac{J_c - (\sigma T_c^4)}{R_3} + h_c A_c (T_{gas} - T_c) - h_{co} A_c (T_c - T_{amb}) - \epsilon_c A_c \sigma (T_c^4 - T_{amb}^4) \quad (3)$$

This accounts for radiant exchange occurring in the space, internal convective gains from the gas, external convection, and radiation. The cold boundary was assumed to cool convectively and radiatively to a quiescent ambient atmosphere. By applying an explicit difference formulation to differential Eq. 3 (using the cold boundary temperature, T_{CO}, from the previous time step), Eq. 3 becomes

$$\frac{A_c \Delta_x \rho C_p (T_{co} - T_c)}{\Delta t} + \frac{J_c - (\sigma T_{co}^4)}{R_3} + h_c A_c (T_{gas} - T_{co}) + h_{co} A_c (T_{amb} - T_{co}) + \epsilon_c \sigma A_c (T_{amb}^4 - T_{co}^4) = 0 \quad (4)$$

The radiant exchange between the hot boundary, cold boundary, and gas is described by a radiation electrical network, which is presented in Fig. 2. The radiation network was used to write an equation for each surface radiosity, J_h and J_c, through an application of Kirchoff's current law. The heat flow in and out of the nodes for J_h and J_c, with the blackbody emissive powers of the hot wall (E_h), cold wall (E_c), and gas (E_g) as source terms, must sum to zero.

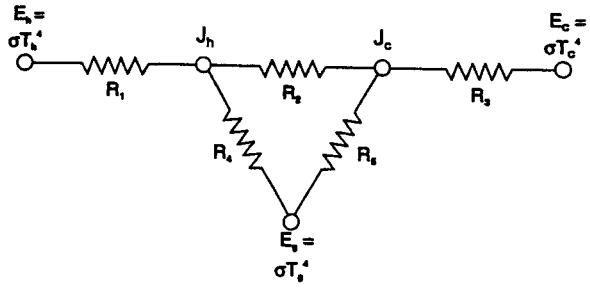

Figure 2. Radiation network.

$$\frac{E_h - J_h}{R_1} + \frac{J_c - J_h}{R_2} + \frac{E_g - J_h}{R_4} = 0 \quad (5)$$

$$\frac{J_h - J_c}{R_2} + \frac{E_g - J_c}{R_5} + \frac{E_c - J_c}{R_3} = 0 \quad (6)$$

where

$$R_1 = \frac{1 - \epsilon_h}{\epsilon_h A_h} \qquad R_2 = \frac{1}{A_h F_{hc} (1 - \epsilon_g)}$$

$$R_3 = \frac{1 - \epsilon_c}{\epsilon_c A_c} \qquad R_4 = \frac{1}{A_h \epsilon_g} \qquad R_5 = \frac{1}{A_c \epsilon_g}$$

Equations 5 and 6 were used with conservation of energy equations for the gas (Eq. 2) and cold boundary (Eq. 4) as a set of simultaneous equations to solve for the four unknowns: J_h, J_c, T_{gas}, and T_c. This system of nonlinear, multivariate equations was solved by the implementation of a Newton-Rapheson method for nonlinear systems of equations. For each time step iteration, the new hot boundary temperature is generated, and the values from the previous time step are used as the initial guesses for the solver.

The cold boundary differential equation is the only equation that has a heat capacity term. Thus, the cold boundary temperature is the only unknown that is directly affected by thermal lag; the other unknowns respond immediately to the changes in the hot wall temperature function.

Input variables and modeling parameters are summarized in Table 1. Input variables are modified on a case by case basis. The modeling parameters identified in Table 1 were fixed through the modeling comparisons with small-scale test data.

Table 1. Input Variables and Modeling Parameters

Input Variables	Modeling Parameters
"Hot" wall temperature history (T_h versus t)	"Hot" wall convective heat transfer coefficient (h_h)
Area of "hot" wall (A_h)	Internal "cold" wall convective heat transfer coefficient (h_c)
Area of "cold" wall (A_c)	External "cold" wall convective heat transfer coefficient (h_{co})
Steel properties (C_p, Δ_x, ρ)	"Hot" wall emissivity (ϵ_h)
Ambient temperature (T_{amb})	"Cold" wall emissivity (ϵ_c)
	Compartment gas emissivity (ϵ_g)

Small-Scale Comparisons and Model Development

Two sources of experimental data were used in this work: post-flashover fires in simulated shipboard compartments[18,19] and post-flashover fires that were performed on the ex-USS SHADWELL in conjunction with other studies.[20–22] These test series focused primarily on the fire compartment and effects on adjacent spaces.

A primary objective of the "Phase I Small-scale Studies" test series[18] was to design a post-flashover fire that could be used in actual shipboard tests. A secondary objective was to develop preliminary estimates of the impact of post-flashover compartment fires on adjacent compartments. The tests were performed in a mock-up constructed of 0.95 cm (3/8 in.) thick steel consisting of an array of four compartments measuring 2.4 × 2.4 × 2.4 m (8 × 8 × 8 ft). The mock-up was arranged with one compartment directly over the burn compartment and compartments located laterally on either side of the burn compartment. All four compartments were well instrumented, and the available data pertaining to adjacent spaces included the exposed bulkhead/deck temperature, air temperatures, and unexposed bulkhead temperatures. The gas (air) temperatures were measured in the center of the compartment by a thermocouple tree with Type K glass-braided thermocouples located every 0.3 m (1 ft) beginning 0.15 m (0.5 ft) off the deck. The unexposed bulkhead temperature was measured by four Type K surface-mounted thermocouples on the bulkhead directly opposite (farthest distance) the exposed bulkhead. These four thermocouples were located in the center of the bulkhead using a 0.61 m (2 ft) spacing beginning 0.3 m (1 ft) above the deck.

The model requires specification of both the hot and "cold" wall emissivities. The emissivities for the hot and cold walls were chosen to be equivalent based on their similarities in material and surface condition. Modeling comparisons were made with small-scale test data assuming the compartment gas emissivity was equal to zero, which simulates a transparent gas. This allowed the wall emissivities to be expressed as a resultant emissivity which is described by Eq. 7.

$$\epsilon_R = \frac{1}{\left(\frac{1}{\epsilon_h} + \frac{1}{\epsilon_c} - 1\right)} \qquad (7)$$

In general, surface emissivities for steel range from 0.24 to 0.85.[27] Three resultant emissivities were chosen to span the range of plausible steel surface emissivities. The specific heat, c_p, of steel was taken as 473 J/kgK, and the density was taken as 7800 kg/m^3 throughout the reported work. The comparison of modeling predictions for the resultant emissivities with data for the West compartment are shown in Figs. 3 and 4, where h_h = 10 W/m^{3}K, h_c = 5.2 W/m^{2}K, and h_{co} = 4.4 W/m^{3}K. All three predictions fall within the compartment gas temperatures (measured at various elevations) in Fig. 3. The shape of the prediction for e_R = 0.4 is nearly identical in shape to the middle two thermocouples of the thermocouple trees measuring the air/gas temperature. Figure 4 indicates that the lowest resultant emissivity of 0.4 (individual emissivities of 0.57) yields the most realistic prediction of the cold wall temperatures (measured at various eleva-

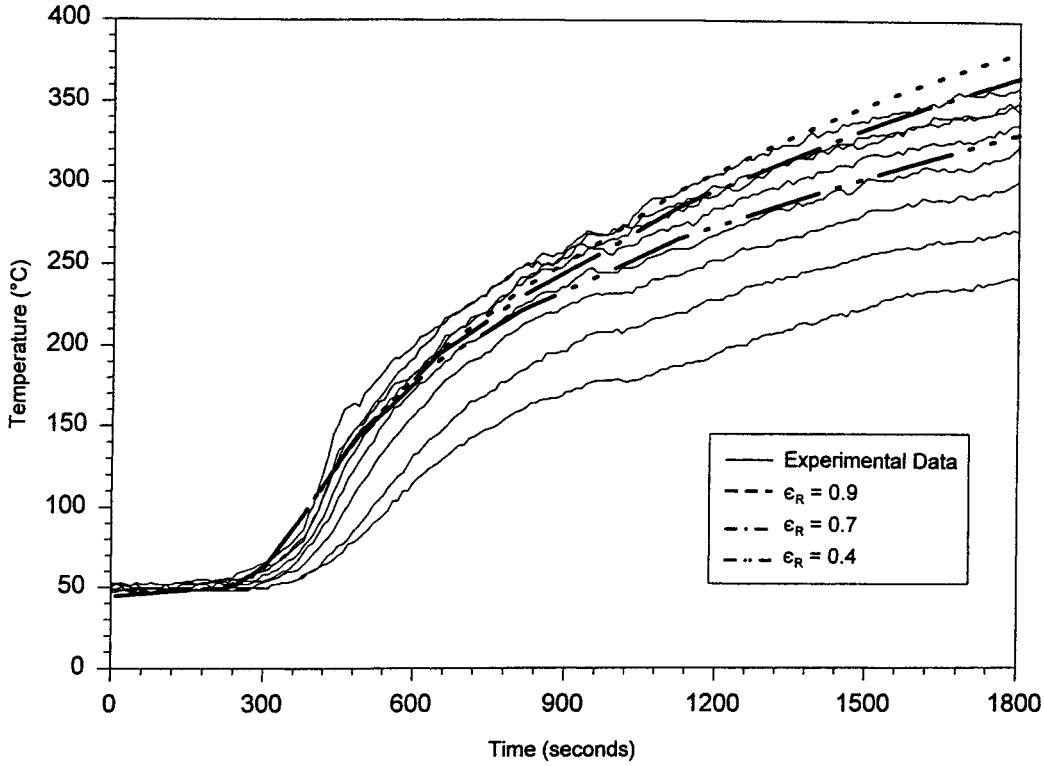

Figure 3. Comparison of modeled compartment gas temperature vs. experimentally measured west compartment gas temperatures: effects of resultant emissivity.

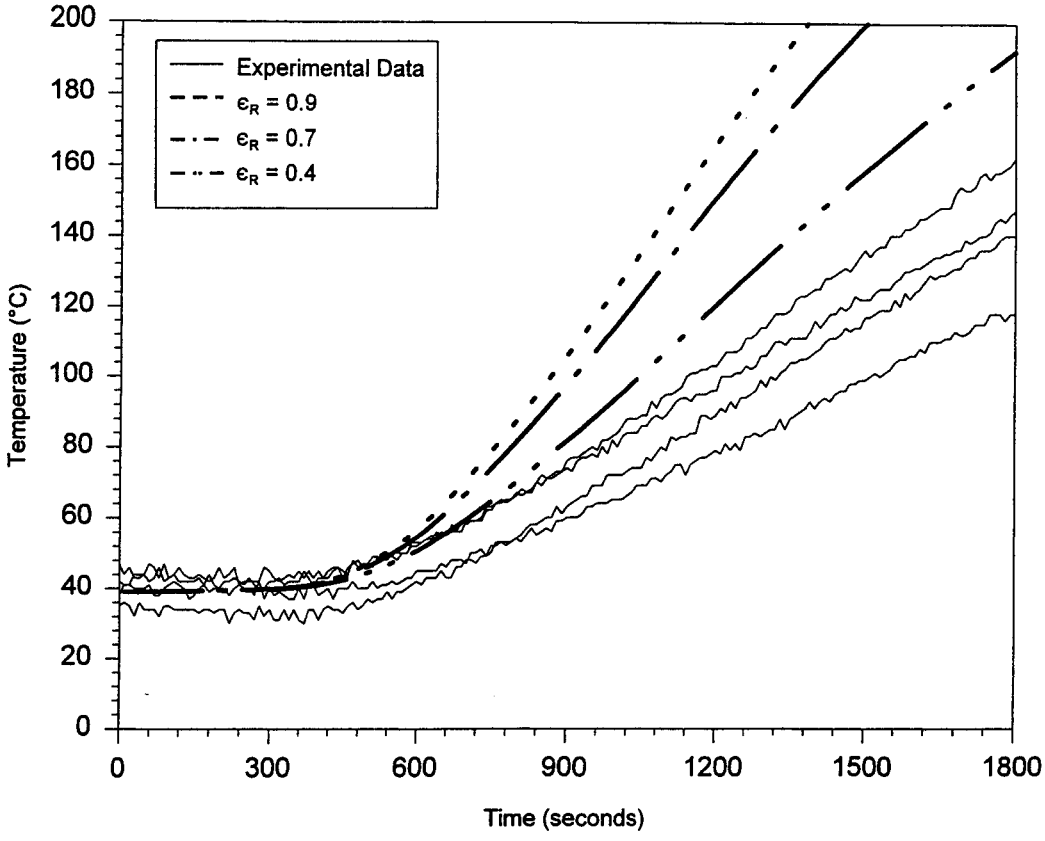

Figure 4. Comparison of modeled wall temperature vs. experimentally measured west wall temperatures: effects of resultant emissivity.

tions). Although the $e_R = 0.4$ conservative prediction is high, it follows the general trend of the cold wall temperatures measured. The individual wall emissivities were fixed at 0.57, yielding the resultant emissivity of 0.4 for the case where the compartment gas is transparent. Individual values of 0.57 are within the range of reported steel emissivity values and are almost identical to the emissivity cited for red, oxidized steel of 0.61.[27]

The model includes three different convective heat transfer coefficients: one for the hot wall, the internal cold wall, and the external cold wall. The internal and external cold wall heat transfer coefficients were estimated based on calculations made for natural convection heat transfer on flat plates in various orientations.[28] Since a single cold wall convective heat transfer coefficient (one coefficient for internal and one for external convective heat transfer) had to characterize heat transfer for five surfaces, an average that accounts for five different surfaces was used. The average value for the external cold wall convective heat transfer coefficient was estimated at 4.4 W/m^2K. This, of course, assumes a quiescent atmosphere to which the external walls are exposed. The average value for the internal cold wall convective heat transfer coefficient is slightly higher than the external cold wall value. The difference accounts for recirculating flows and possible ceiling jets that may be formed from a hot bulkhead/overhead plume. The internal cold wall heat transfer coefficient was estimated to be 5.2 W/m^2K. These two coefficients will have a large impact on the dissipation of thermal energy from the adjacent compartment.

The convective heat transfer coefficient for the hot wall significantly impacts the gas temperature predictions in the adjacent space. Simple hand calculations and engineering approximations indicate that a convective heat transfer coefficient in the range of 7 to 14 W/m^2K is appropriate.[28] A sensitivity analysis was performed using 7, 10, and 14 W/m^2K as the hot wall heat transfer coefficients with a resultant emissivity of 0.4. Comparison of model predictions with compartment gas temperatures and cold wall temperatures measured at various elevations are shown in Figs. 5 and 6. A hot wall convective heat transfer coefficient of 10 W/m^2K was selected since it resulted in the best average gas temperature prediction. Figure 6 illustrates that the hot wall convective heat transfer coefficient has little impact on the cold wall temperature predictions. This indicates that the radiant heating mechanism dominates the prediction of the cold wall temperature.

The gas emissivity is dependent on the compartment size and the quantity of smoke in the space. Pyrolysis of bulkhead and deck surface coatings could affect the gas emissivity. This potentially important variable has complicated dependencies and is not easily predicted. Results of the analysis show that the predictive capabilities of the model are relatively insensitive to the gas emissivity, which is reflected in Figs. 7 and 8. Figure 7 shows that the gas emissivity is best modeled as being transparent (gas emissivity of zero) to obtain the best predictions of gas temperatures. Figure 8 shows the effect of the gas emissivity on the wall temperatures; the wall temperatures decrease slightly as the gas emissivity increases due to the gray gas absorption of some of the radiant energy leaving the hot wall. The emissivity of the gray gas was set to zero for the blind predictions of the large-scale tests. This is consistent with visual observations of the adjacent spaces and distinct lack of bulkhead/deck surface treatments in adjacent spaces in these tests.

Modeling predictions have been compared to small-scale data in order to define the modeling parameters. These modeling parameter values have been fixed and are summarized in Table 2. These parameter values remain fixed for the blind large-scale test modeling.

RESULTS

Several test series involving post-flashover fires in a shipboard compartment have been performed on the ex-USS SHADWELL.[20-22] These test series were used to determine stoichiometric fire sizes and evaluate cooling of bulkheads, venting of adjacent spaces, and the insulation of bulkheads and decks. The test configuration included eight compartments each measuring approximately 8.5 × 3.7 × 3.1 m (28 × 12 × 10 ft) and arranged as in Fig. 9. Post-flashover conditions were generated in Berthing 2 by diesel fuel spray fires. Berthing 1 and 2 represented living quar-

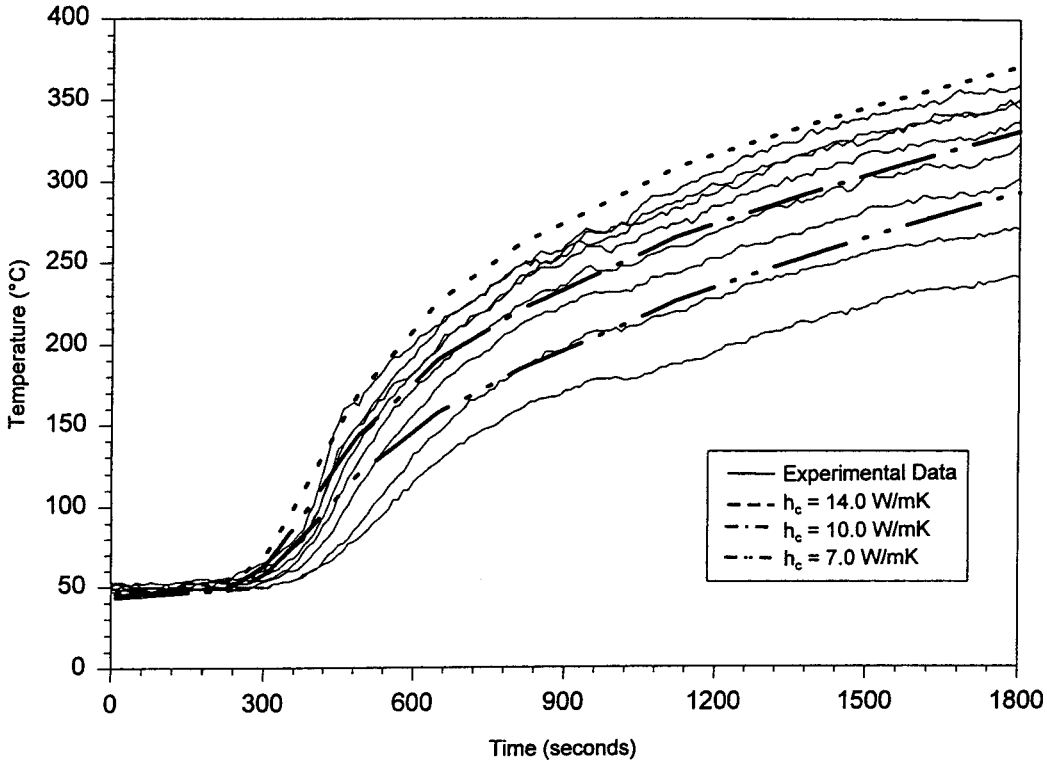

Figure 5. Comparison of modeled compartment gas temperature vs. experimentally measured west compartment gas temperatures: effects of hot wall convection coefficient.

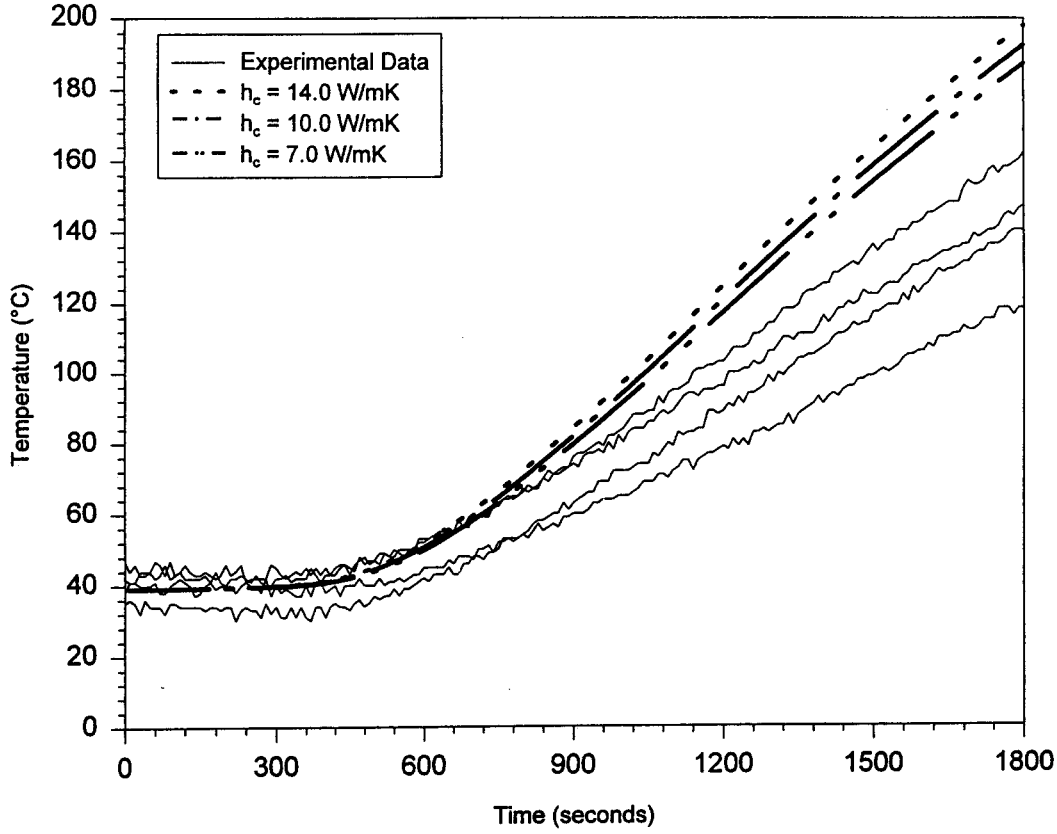

Figure 6. Comparison of modeled compartment wall temperature vs. experimentally measured west wall temperatures: effects of hot wall convection coefficient.

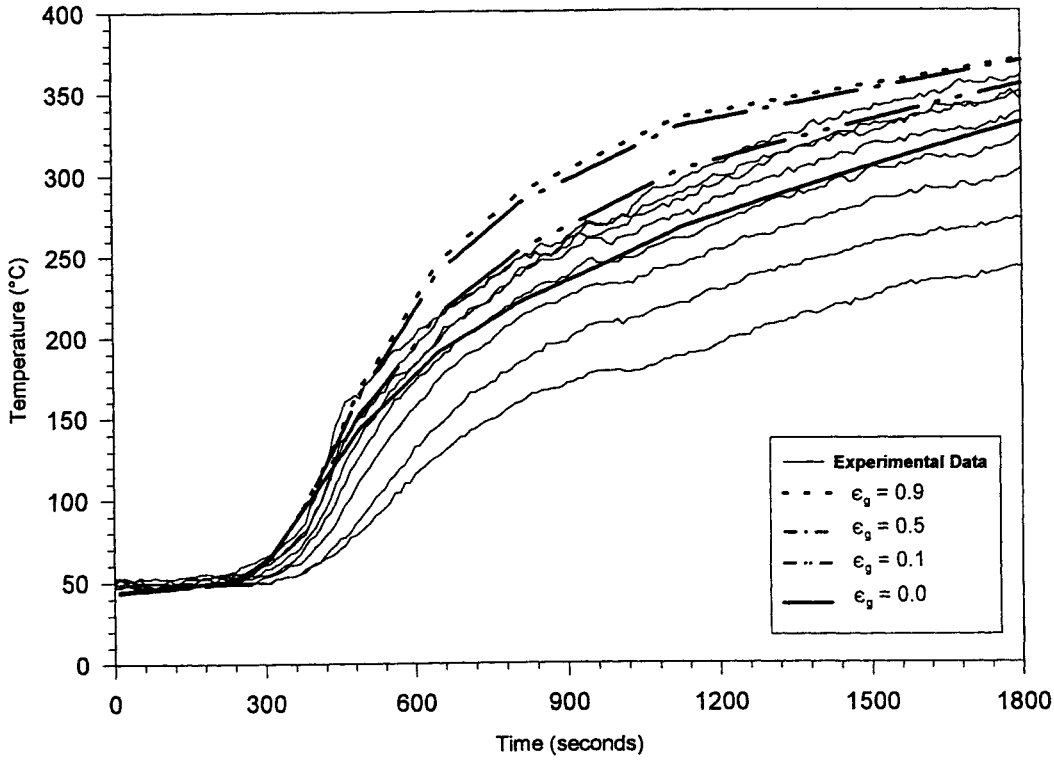

Figure 7. Comparison of modeled compartment gas temperature vs. experimentally measured west compartment gas temperatures: effects of gas emissivity.

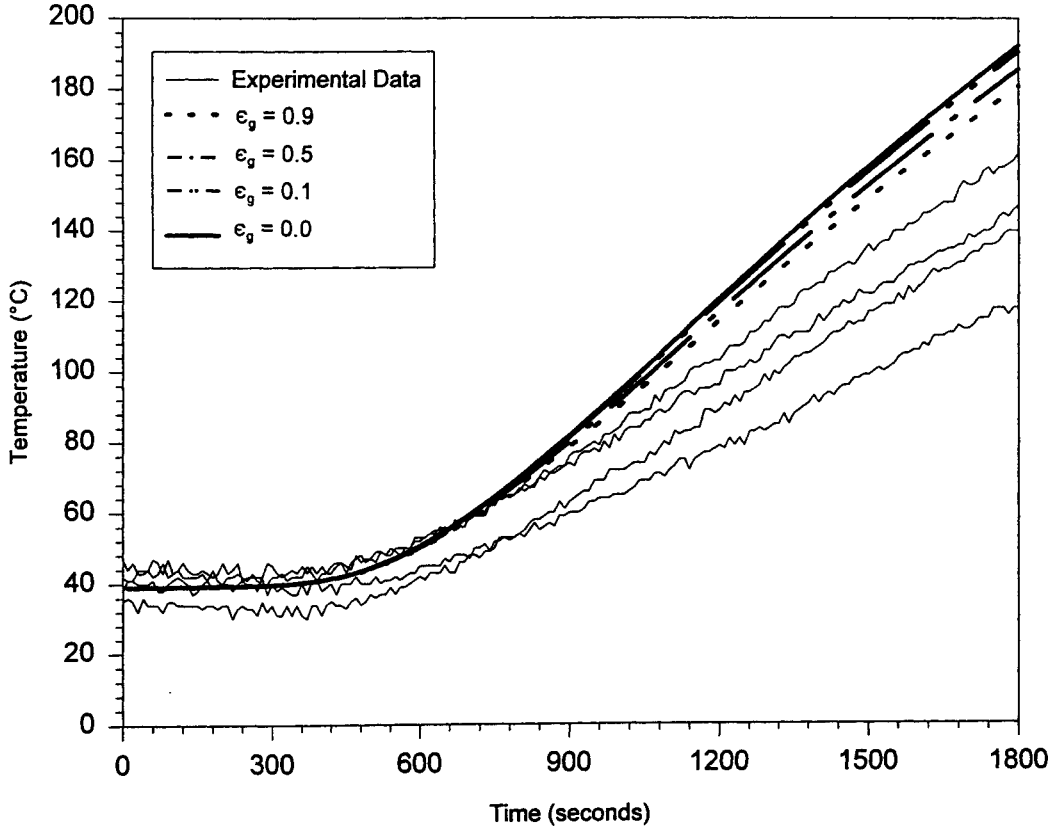

Figure 8. Comparison of modeled wall temperature vs. experimentally measured west wall temperatures: effects of gas emissivity.

Table 2. Final Values for Modeling Parameters

Modeling Parameters	Final Values
"Hot" wall convective heat transfer coefficient	h_h = 10.0 W/m^{2}K
Internal "cold" wall convective heat transfer coefficient	h_c = 5.2 W/m^{2}K
External "cold" wall convective heat transfer coefficient	h_{co} = 4.4 W/m^{2}K
"Hot" wall emissivity	ϵ_h = 0.57
"Cold" wall emissivity	ϵ_c = 0.57
Compartment gas emissivity	ϵ_g = 0.0

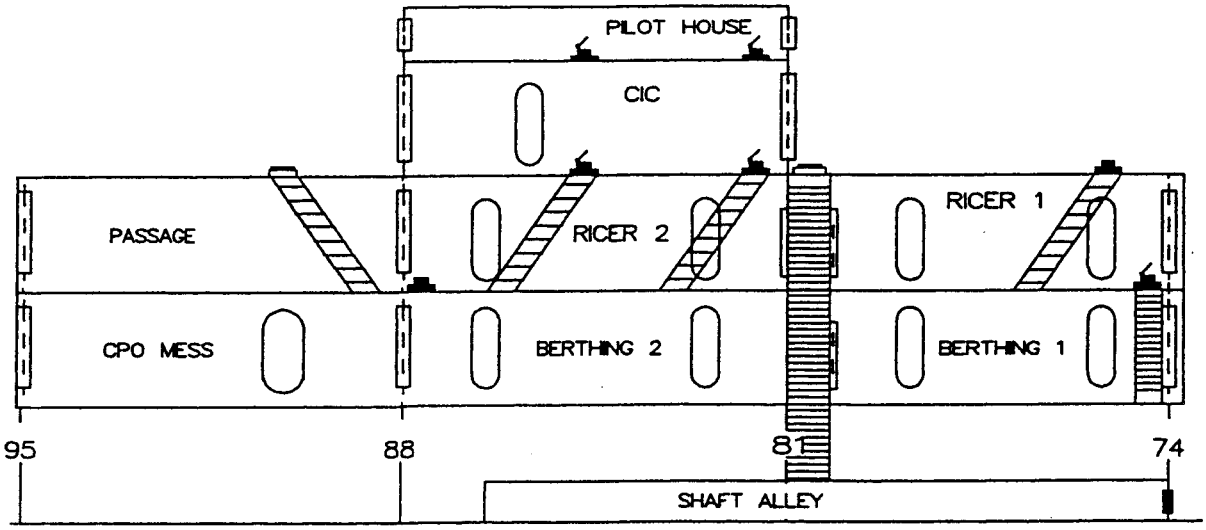

Figure 9. Compartment arrangement for full-scale tests.

ters, RICER 2 represented an electronics space, and CPO Mess represented a dining area. Data from RICER 2, Berthing 1, and the CPO Mess were used in this study. Data similar to those recorded in the small-scale studies were obtained: air temperatures at various heights in the compartment, total heat flux levels, and exposed/unexposed bulkhead and deck temperatures. Gas temperatures were measured in RICER 2 with glass-braided Type K thermocouples in a vertical string at 0.4, 0.9, 1.4, 1.8, and 2.3 m above the deck. Only two thermocouples were used in the CPO Mess to measure the gas temperatures at 0.9 and 2.3 m above the deck. The bulkhead temperatures used for comparison for RICER 2 were surface mounted, glass-braided Type K thermocouples located (1) on the underside of the overhead in RICER 2 and (2) on the aft transverse bulkhead at 0.9 and 0.15 m above the deck.

Predictions for various scenarios from the full-scale ex-USS SHADWELL[22] tests were made without altering modeling parameters established in Table 2. A test that yielded average comparative results has been included and discussed. For RICER 2 and CPO Mess, two spaces adjacent to Berthing 1, the unexposed thermocouples of the "hot" bulkhead were plotted, and a reasonable input function for the hot boundary temperature was derived. Figure 10 shows the hot wall temperature history for RICER 2. Figure 11 shows the hot wall thermocouple data for CPO Mess at 0.9 and 1.5 m above the deck. This hot wall temperature history and the remaining input variables were updated for each adjacent space that was modeled. The thermal impact on all three adjacent spaces (RICER 2, Berthing 1, and CPO Mess) was simulated.

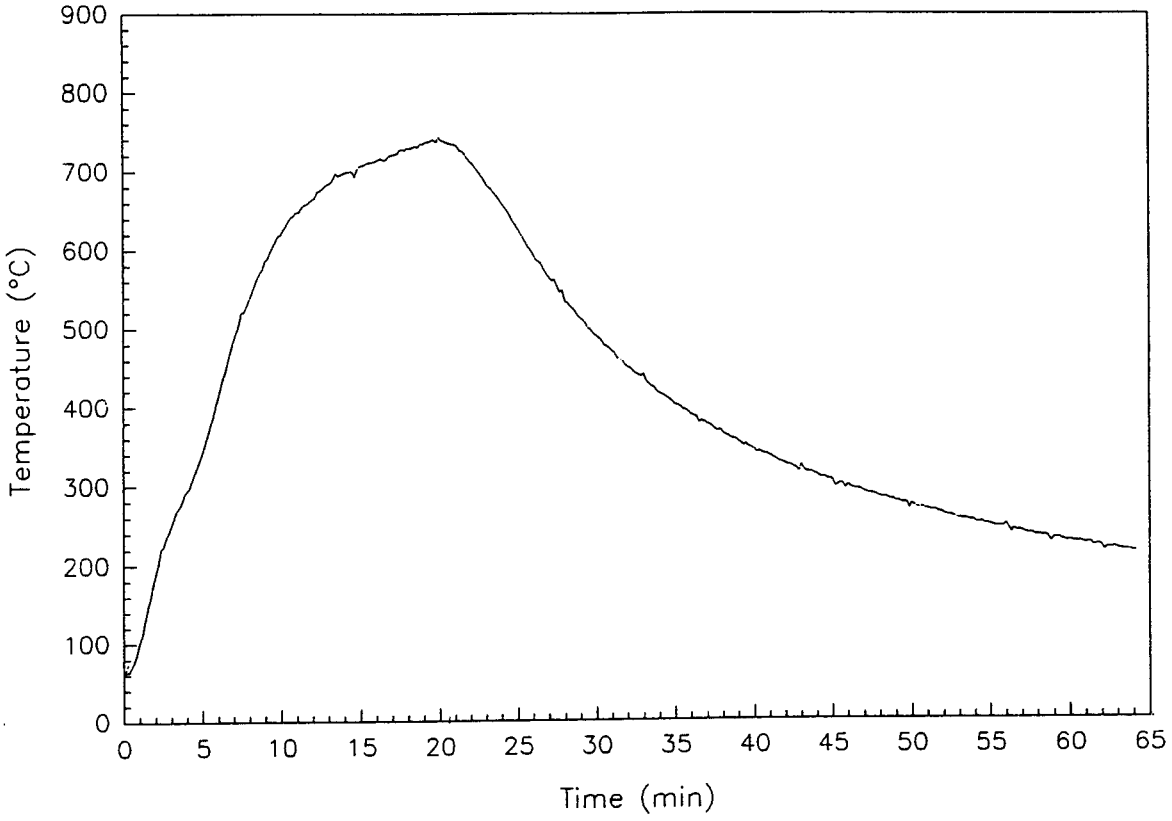

Figure 10. Hot wall temperature history for RICER 2.

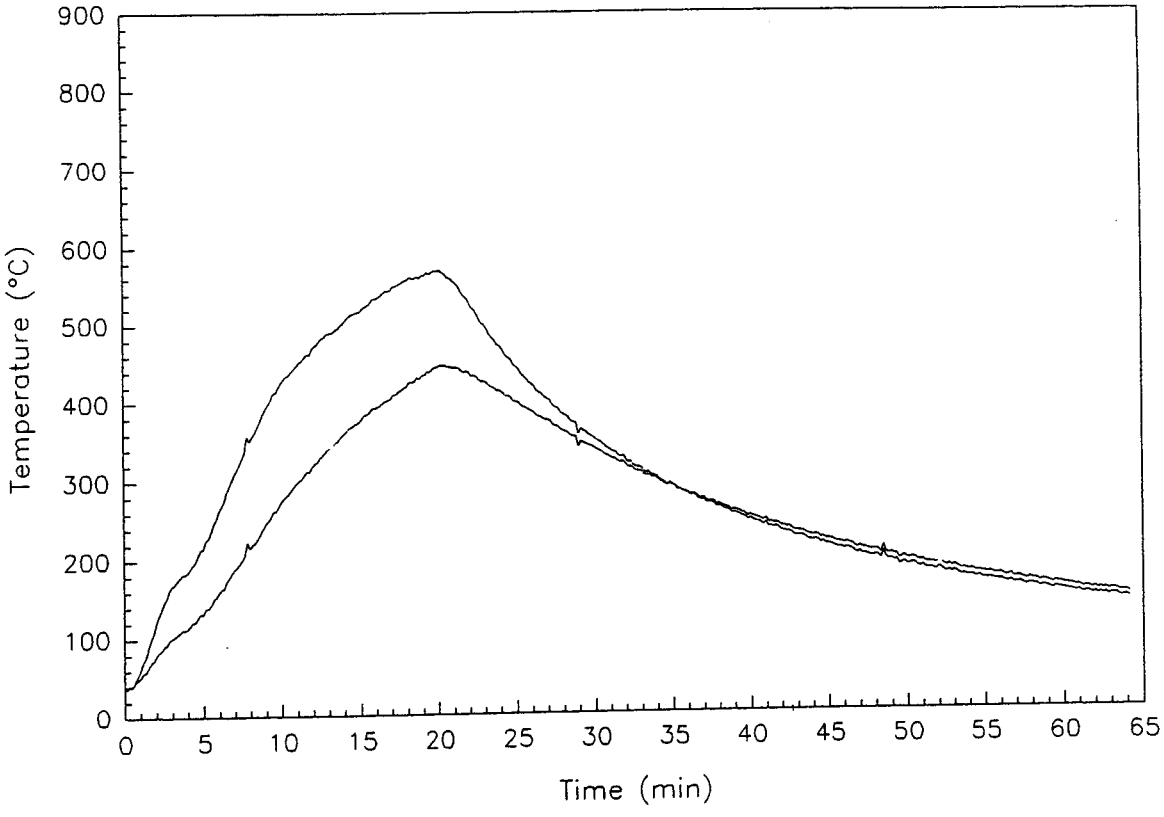

Figure 11. Hot wall temperature history for CPO Mess.

In all full-scale test simulations, the gas temperature predictions in the adjacent space are slightly higher than the data recorded describing the thermal environment in the space. This is reflected in Fig. 12, which shows the results for RICER 2, and in Fig. 13, which shows the results for the CPO Mess. Overpredictions by the model were expected since the model parameters were developed to yield conservative estimates. This would translate into either shorter times of tenability or faster times to ignite Class A materials in adjacent spaces. The entire hot wall surface was assumed to be at the recorded temperature of the thermocouple that was located in the center of the bulkheads—often preferentially exposed to the effects of post-flashover fires. The spray fires were geometrically centered, and thermocouples located near the center of the bulkheads would not necessarily reflect the average bulkhead temperature. The shapes of the gas temperature predictions are remarkably similar in shape to the experimental data, often offset by a small margin.

The cold boundary temperature predictions are systematically high in comparison to both the small-scale and the full-scale shipboard test results. The predicted cold boundary temperature for RICER 2 was compared with several thermocouples in Fig. 14, which illustrates the overprediction by the model. Comparisons for the lateral compartments (not shown), CPO mess and Berthing 1, also exhibit higher model predictions than full-scale test data. The temperature increase of the cold walls in the lateral compartments is minimal, approximately 20°C, while the model predicts a temperature increase of 30°C. The lateral compartment overprediction may be attributable, in part, to the data used in these comparisons. The two horizontally adjacent spaces, Berthing 1 and the CPO Mess, were instrumented with a single thermocouple located on the bulkhead farthest from the hot boundary, which could characterize the cold wall thermal response. Differences could result since the model predicts an average cold boundary temperature for the other five surfaces and it was compared with a thermocouple measuring a bulkhead temperature in one of the colder areas of the five surfaces. The conservative nature of the model introduces other factors that contribute to overpredicting the cold boundary temperatures;

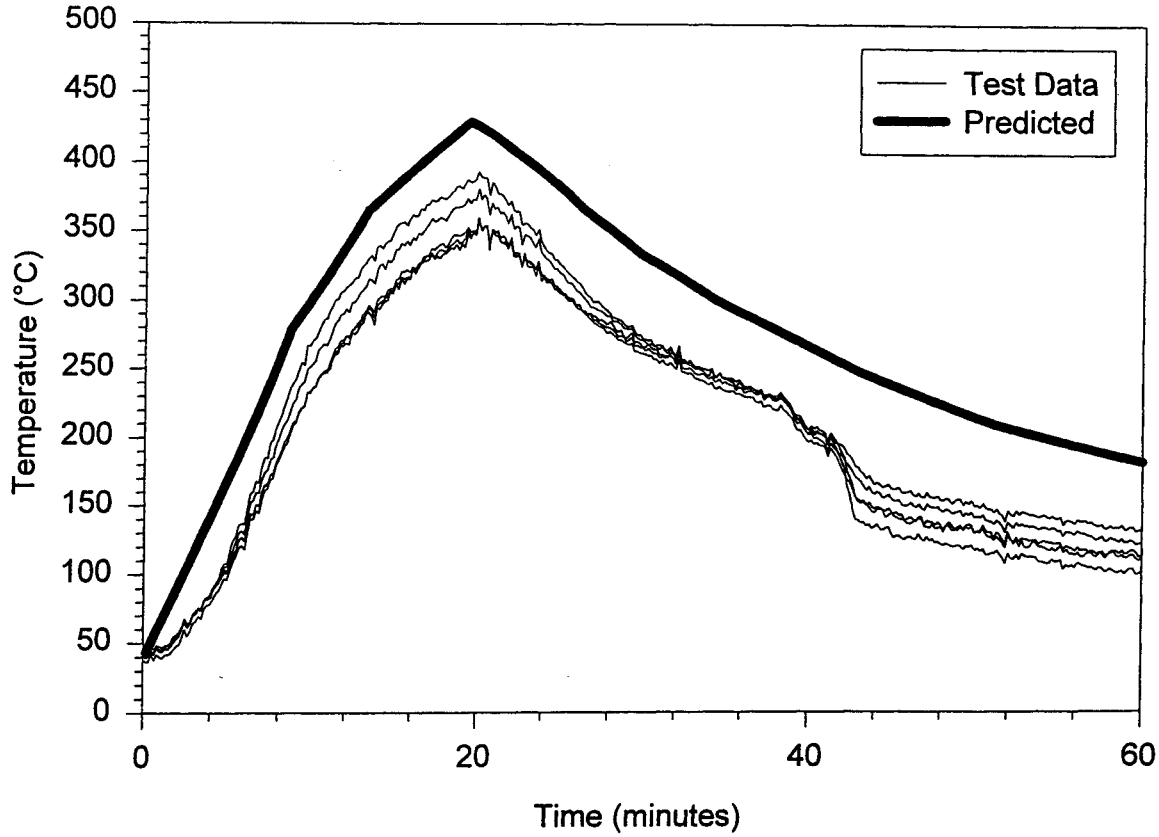

Figure 12. Gas temperatures for RICER 2: predicted vs. full scale.

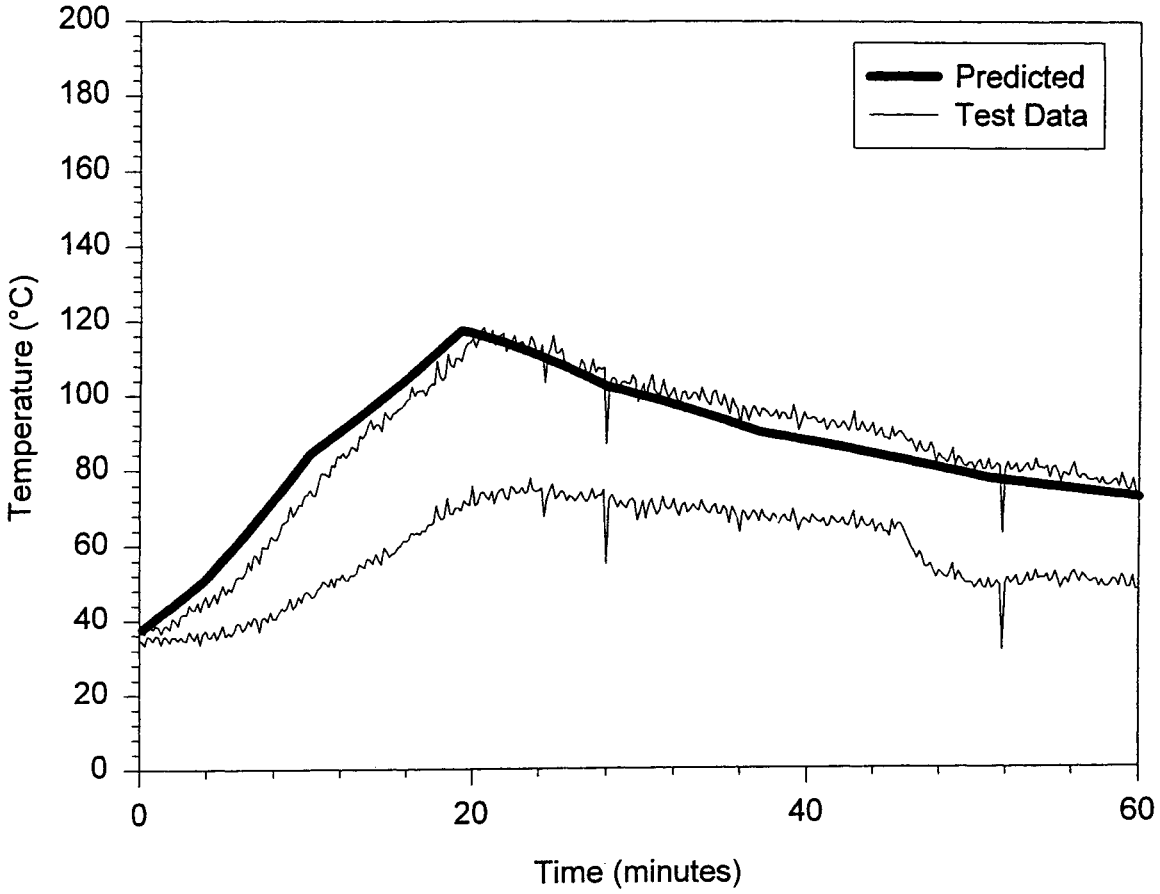

Figure 13. Gas temperatures for CPO Mess: predicted vs. full scale.

these include high predictions of the gas temperature, which increases the level of radiant energy, and use of an average external heat transfer coefficient, which was calculated for a quiescent atmosphere.

Equations 2 and 4 can be manipulated to expose the dimensionless parameter of the hot boundary area divided by the cold boundary area. This dimensionless parameter is obtained in Eq. 2 by substituting expressions for R_4 and R_5 and dividing through by the cold boundary area. The ratio is embedded in Eq. 2 in the J_c term. This is an intuitively important parameter as the hot wall area governs the amount of energy transferred into the adjacent space, and the cold boundary area governs the heat lost from the space. The small-scale shipboard compartments[19] yielded an A_h/A_c = 0.2 for each of the adjacent spaces. The shipboard tests[22] yielded various A_h/A_c values depending on the adjacent space selected. The range of A_h/A_c values, from 0.06 for Berthing 2 to 0.31 for RICER 1, yielded modeling results which are consistent over this wide range of A_h/A_c values. It can be concluded that the accuracy of the model is insensitive to the ratio of hot wall area to cold wall area.

Since the A_h/A_c ratio governs the heat loss and gains for the adjacent space, there must be a relationship between the area ratios and the thermal impact on adjacent spaces. Figure 15 reflects the relationship between the hot wall and cold wall areas ratio and thermal effects in adjacent compartments according to this model. The data reflected in Fig. 15 are based on multiple model runs. The inputs were identical with the exception of the hot and cold wall area values. The modeling parameters from Table 2 were used. The hot wall temperature history was based on full-scale test data for the RICER 2 deck. This was the most extreme temperature history of all tests simulated. The hot and cold wall areas were manipulated to cover the area ratios, and the gas temperature of the adjacent compartment was recorded at 15 and 20 minutes. The 15- and 20-minute time frames are benchmarks associated with initiating active

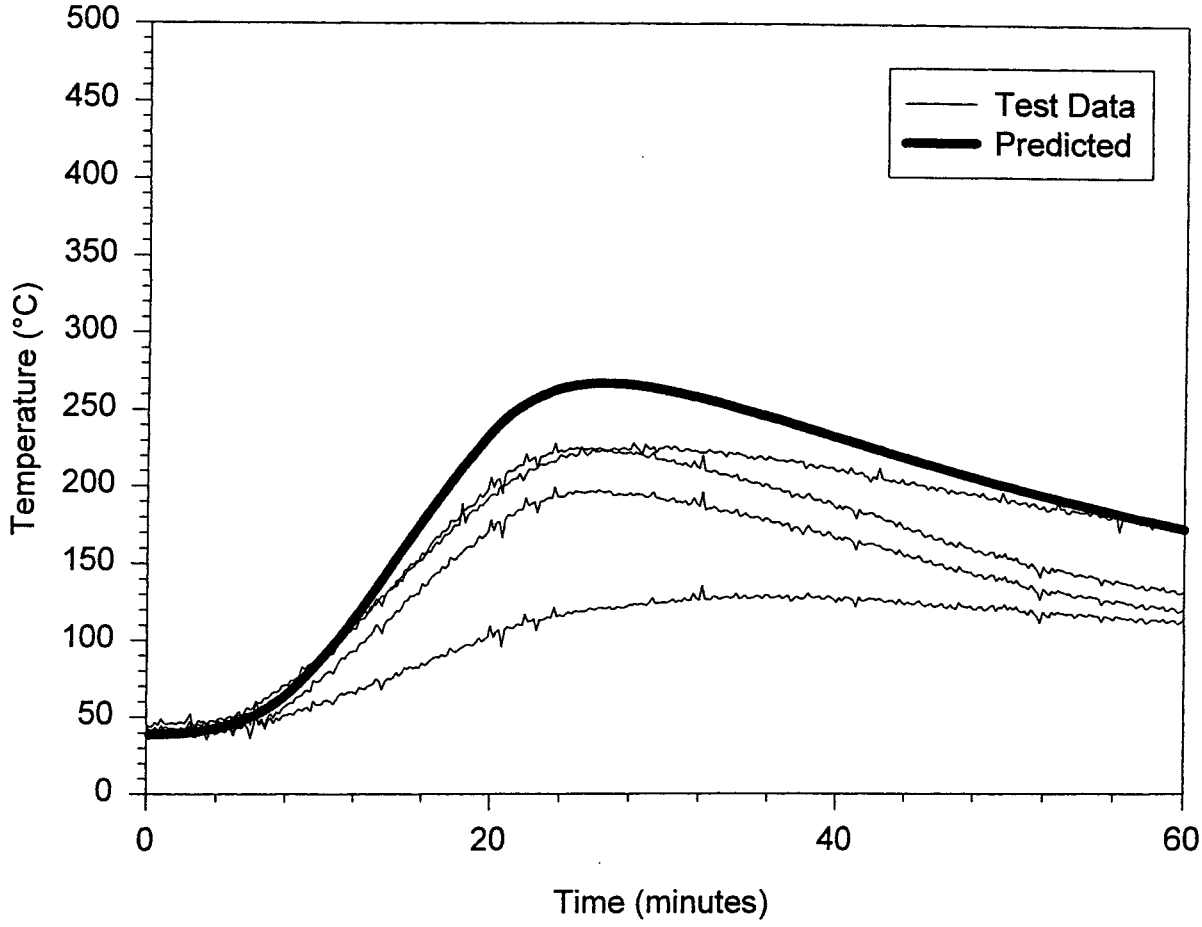

Figure 14. Bulkhead temperatures for RICER 2: predicted vs. full scale.

shipboard firefighting and damage control activities. Two thresholds appear in Fig. 15 that address concerns relating to human tenability, susceptibility of electronic equipment, and ignition of ordinary combustibles. The threshold values for these concerns are based on reported values in the Navy Ships' Technical Manual[29] and are summarized in Table 3. Figure 15 translates, practically, to the conservative assessment that, in a 20-minute time frame, the area ratio must be 0.05 or less to avoid computer equipment damage and human tenability problems, and must be 0.11 or less to avoid pilotless ignition of paper on a short time frame.

Conclusions

The rationale and theoretical development of a predictive model that calculates the thermal environment in a space adjacent to a post-flashover fire has been described. Conservative and representative predictions of the thermal environment have been made as compared with small- and full-scale testing. Small-scale comparisons were used to define model parameters that were fixed for large-scale predictions. The results show that for reasonable estimations of the hot common surface, a conservative estimate can be calculated for the gas and wall temperatures in the space as a function of time for large-scale applications. The qualitatively good predictive capabilities of the model are based on model parameters that were fixed from small-scale comparisons. From these predictions, tenability in the adjacent space and the development of fire spread through the ignition of ordinary combustibles can be determined.[29,30]

Several interesting observations have been made. An important result is the relative insensitivity of the model to the emissivity of the gray gas. This is fortunate as it would be very difficult to predict the gray gas emissivity in an adjacent space with any accuracy. The best comparative

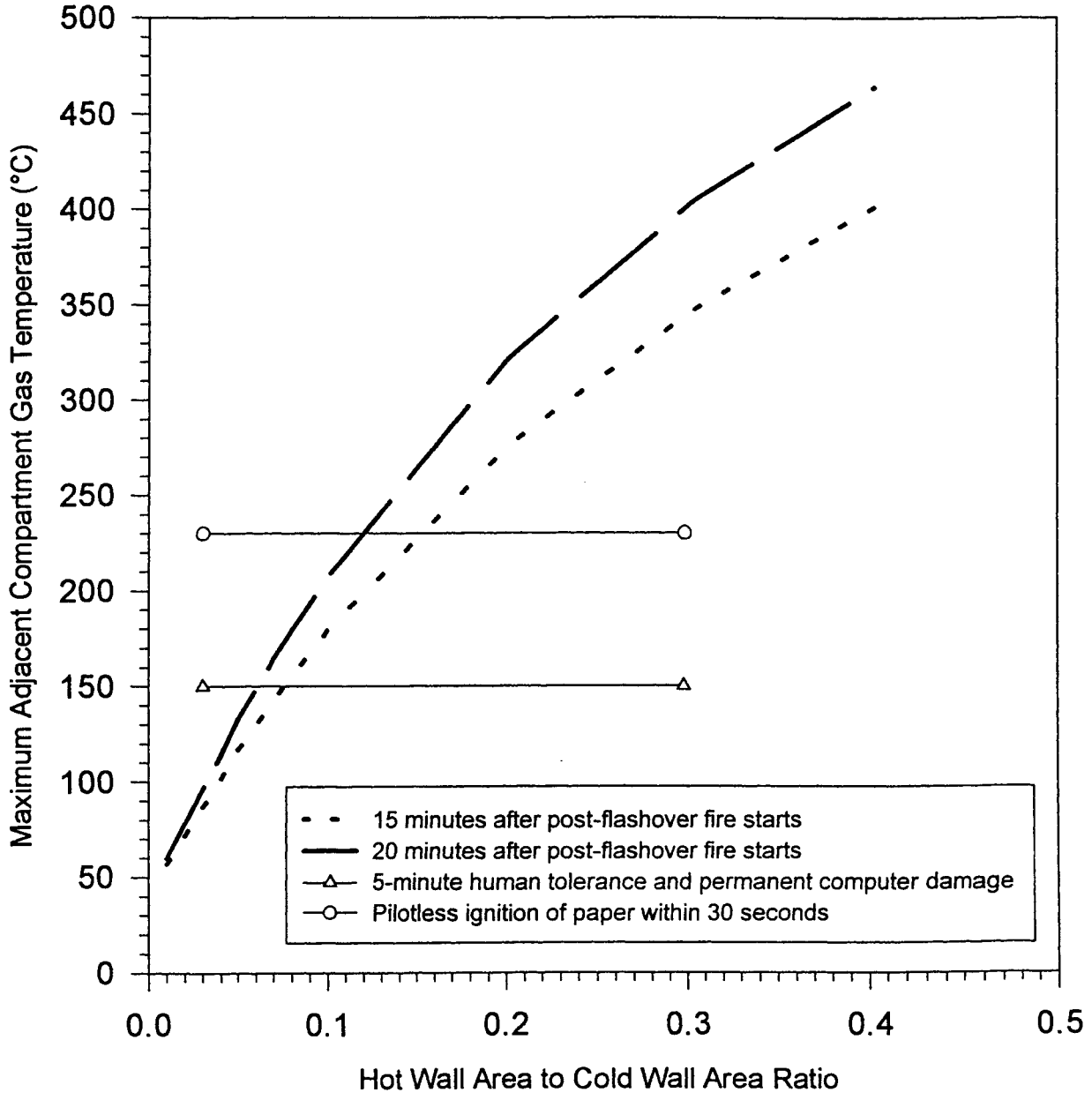

Figure 15. Relationship between hot wall and cold wall area ratio and thermal effects in adjacent compartments.

Table 3. Thermal Effects and Threshold Values[29]

Thermal Effect	Threshold Value
Human tenability—incapacitation in 5 minutes	149°C
Permanent computer damage	150°C
Pilotless ignition of paper within 30 seconds	230°C

results were obtained by using a gray gas emissivity of zero, which represents a transparent gas that does not participate in the radiant exchange. This also reflects a very conservative perspective for a transparent gas that allows the maximum predicted incident radiant flux. This translates to more rapid ignition times for remote Class A materials and shorter tenability times for persons who would be exposed to elevated gas temperatures. Personnel and materials would be heated at the maximum rate as there would be no "smoke" shield to reduce thermal radiation.

The comparisons between the model and experimental data show conservative predictions. This is attributed to an overestimation of the average hot wall temperature and underestimating the external convective losses because of wind effects[22] on the experimental results.

NOMENCLATURE

A_c = cold wall surface area (m^2)
A_h = hot wall surface area (m^2)
C_p = specific heat of gases, steel (J/kg K)
E_c = blackbody emissive power of cold walls (W)
E_g = blackbody emissive power of compartment gas (W)
E_h = blackbody emissive power of hot wall (W)
F_{hc} = view factor for radiation from the hot to cold walls
h_c = cold wall convection heat transfer coefficient in the compartment (W/m^2K)
h_{co} = cold wall convection heat transfer coefficient outside the compartment (W/m^2K)
h_h = hot wall convection heat transfer coefficient in the compartment (W/m^2K)
J_c = radiosity of the cold wall
J_h = radiosity of the hot wall
R_1–R_5 = radiative resistance
T_{amb} = ambient temperature (K)
T_c = cold wall temperature (K)
T_{co} = cold wall temperature at previous time step (K)
T_{gas} = compartment gas temperature (K)
T_h = hot wall temperature (K)
t = time (s)
V = volume (m^3)
Δ_x = cold wall thickness (m)
ϵ_c = cold wall emissivity
ϵ_g = compartment gas emissivity
ϵ_h = hot wall emissivity
ϵ_R = resultant emissivity
ρ = density (kg/m^3)
σ = Stefan-Boltzmann constant ($5.67 \times 10^{-8} W/m^2K^4$)

REFERENCES

1. Kawagoe, K., "Fire Behavior in Rooms," Building Research Institute, Report No. 27, Tokyo, 1958.

2. Thomas, P.H., and Heselden, A.J.M., "Fully Developed Fires in Single Compartments. A Cooperative Research Programme of the Conseil Internationale du Batiment," Conseil Internationale du Batiment, Report No. 20, Fire Research Note 923, 1972.

3. Thomas, P.H., Heselden, A.J.M., and Law, M., "Fully Developed Compartment Fires: Two Kinds of Behavior," Fire Research Technical Paper, No. 18, HMSO, London, 1967.

4. Croce, P.A. (ed.), "A Study of Room Fire Development: The Second Full-scale Bedroom Fire Test of the Home Fire Project," Factory Mutual Research Corporation Serial 21011.4, RC 75—T 31, Norwood, MA, 1975.

5. Harmathy, T.Z., "A New Look at Compartment Fires," Parts I and II, *Fire Technology*, Vol. 8, 1972, Part I–pp. 196–219; Part II–pp. 326–351.

6. Harmathy, T.Z., "Mechanism of Burning of Fully-developed Compartment Fires," *Combustion and Flame*, Vol. 31, 1978, pp. 256–273.

7. Thomas, P.H., and Nilsson, L., "Fully-developed Compartment Fires: New Correlations of Burning Rates," Fire Research Note No. 657, 1973.

8. Bullen, M.L., "A Combined Overall and Surface Energy Balance for Fully-developed Ventilation Controlled Liquid Fuel Fires in

Compartments," *Fire Research*, Vol. 1, 1977, pp. 171–185.

9. Bullen, M.L., and Thomas, P.H., "Compartment Fires with Non-cellulosic Fuels," *17th Symposium (International) on Combustion*, The Combustion Institute, Pittsburgh, PA, 1979, pp. 1139–1148.

10. Drysdale, D., "The Post-flashover Compartment Fire," Chapter 10 in *An Introduction to Fire Dynamics*, John Wiley & Sons, NY, 1985, pp. 304–350.

11. Bohm, B., "Fully Developed Polyethylene and Wood Compartment Fires with Application to Structural Design," Technical University of Denmark, Laboratory of Heating and Air Conditioning, Denmark, 1977.

12. Kawagoe, K., and Sekine, T., "Estimation of Temperature-time Curves in Rooms," Occasional Report No. 11, Building Research Institute, Tokyo, 1963.

13. Pettersson, O., Magnusson, S.E., and Thor, J., "Fire Engineering Design of Structures," Publication 50, Swedish Institute of Steel Construction, 1976.

14. Babrauskas, V., and Williamson, R.B., "Post-flashover Compartment Fires: Basis of a Theoretical Model," *Fire and Materials*, Vol. 2, 1978, pp. 39–53.

15. Babrauskas, V., and Williamson R.B., "Post-flashover Compartment Fires: Application of a Theoretical Model," *Fire and Materials*, Vol. 3, 1979, pp. 1–7.

16. Babrauskas, V., "A Closed-form Approximation for Post-flashover Compartment Fire Temperatures," *Fire Safety Journal*, Vol. 4, 1981, pp. 63–73.

17. Babrauskas, V., "COMPF2–A Program for Calculating Post-flashover Fire Temperatures," NBS Technical Note 991, National Bureau of Standards, Gaithersburg, MD, 1979.

18. Back, G.G., Fulper, C.R., Ouellette, R.J., Scheffey, J.L., Willard, R.L., and Leonard, J.T., "Post-Flashover Fires in Simulated Shipboard Compartments: Phase II—Cooling of Fire Compartment Boundaries," NRL Memorandum Report 6896, September 19, 1991.

19. Back, G.G., Leonard, J.T., Fulper, C.R., Darwin, R.L., Scheffey, J.L., Willard, R.L., DiNenno, P.J., Steel, J.S., Ouellette, R.J., and Beyler, C.L., "Post-Flashover Fires in Simulated Shipboard Compartments: Phase I—Small Scale Studies," NRL Memorandum Report 6886, September 3, 1991.

20. Back, G.G., Scheffey, J.L., Williams, F.W., Toomey, T.A., Darwin, R.L., and Ouellette, R.J., "Post-Flashover Fires in Simulated Shipboard Compartments—Phase III Venting of Large Shipboard Fires," NRL Memorandum Report NRL/MR/6180-93-7338, June 9, 1993.

21. Scheffey, J.L., Toomey, T.A., Hunt, S.P., Durkin, A.F., Darwin, R.L., and Williams, F.W., "Post-Flashover Fires in Simulated Shipboard Compartments—Phase IV: Impact of Navy Fire Insulation," NRL Memorandum Report NRL/MR/6183-93-7335, June 9, 1993.

22. Williams, F.W., Scheffey, J.L., Hill, S.A., Toomey, T.A., Darwin, R.L., Leonard, J.T., and Smith, D.E., "Post-flashover Fires in Shipboard Compartments Aboard ex-USS SHADWELL: Phase V–Fire Dynamics," NRL/FR/6180-99-9902, May 31, 1999.

23. Bailey, J.L., and Tatem, P.A., "Validation of Fire/Smoke Spread Model (CFAST) Using ex-USS SHADWELL Internal Ship Conflagration Control ISCC Fire Tests," NRL Memorandum Report NRL/MR/6180-95-7781, September 30, 1995.

24. Williams, F.W., Toomey, T.A., and Carhart, H.W., "The ex-SHADWELL Full-scale Fire Research and Test Ship," NRL Memorandum Report 6074, reissued September 1992.

25. Barnett, J.R., Worcester Polytechnic Institute, Worcester MA, personal communication, May 1990.

26. Emmons, H.W., "The Prediction of Fires in Buildings," *Seventeenth Symposium (International) on Combustion*, The Combustion Institute, Pittsburgh, PA, 1978.

27. Eckert, E.R.G. and Draker, R.A., Jr., *Analysis of Heat and Mass Transfer*, McGraw-Hill, Inc., New York, 1972.

28. Atreya, A., "Convective Heat Transfer," *The SFPE Handbook of Fire Protection Engineering*, National Fire Protection Association, Quincy, MA, 1988.

29. Darwin, R.L., Leonard, J.T., and Scheffey, J.L., "Fire Spread by Heat Transmission Through Steel Bulkheads and Decks," *Proceedings of IMAS Conference on Fire Safety on Ships*, Institute of Marine Engineers, London, England, May 1994.

30. Naval Sea Systems Command, "Naval Ships' Technical Manual," S9086-S3-STM-010, Chapter 555, Shipboard Firefighting, First Revision, Naval Sea Systems Command, Department of the Navy, Washington, DC, 1 June 1993.